Electronic Supplementary Material (ESI) for Materials Chemistry Frontiers.

Supporting Information

Nanoconfinement – Amplified, Förster Resonance Energy Transfer in Nile Red - Borne Mesoporous Silica for Ultrasensitive, Multiplex Assay of Triphenylmethane Dyes in Aqueous Milieu

Yifan Chen, Sijian Ye, Chongling Cheng*, Renguo Xie, and Dayang Wang*

State Key Laboratory for Inorganic Synthesis and Preparative Chemistry, College of Chemistry, Jilin University, 130012, Changchun, China.

*Corresponding authors: chengchongling@jlu.edu.cn and wangdayang@jlu.edu.cn

1. Experimental Section

1. 1. Materials

Nile red (NR) and pyrene were purchased from Sigma-Aldrich (Shanghai). Malachite green (MG), brilliant green (BG), methylene blue (MB), methyl blue, 9, 10-bis(phenylethynyl) anthracene, Sudan Red IV, nitrofurazone, tetracycline hydrochloride, chloramphenicol, sulfadiazine and norfloxacin were purchased from Shanghai Aladdin Biochemical Technology Co. Ltd.. Dichloromethane(DCM) and absolute ethanol were purchased from Sinopharm Group, China. All the chemicals were used as received. Water with a resistivity of 18 $M\Omega\cdot cm^{-1}$ was prepared using a Millipore Milli-Q system and used in all experiments. Phosphate buffered saline (PBS) tablets were purchased from Sigma-Aldrich (Shanghai) and PBS solution was prepared by dissolving one PBS tablet in 200 mL of water.

MCM-41 particles (XFNANO-101428) were purchased from Nanjing XFNANO Materials Tech Co., Ltd.; their density was 0.7×10^3 kg/m^3 and their mean sizes was in the range of 1 - 2 μm. Prior to use, the received MCM-41 particles were calcined at 500 °C in air for 2 h to remove organic impurities potentially left over on the particle surfaces and within their mesopores. Subsequently, the calcinated particles were washed with water until the resistivity of the supernatant water was higher than 10 $M\Omega\cdot cm^{-1}$ to ensure complete removal of inorganic and organic impurities. Finally, the resulting MCM-41 particles were thoroughly dried in vacuo at 500 °C for 2 h.

1.2. Methods.

1.2.1. Study of the local polarity of the mesopores of MCM-41 particles. 10 mg of freshly cleaned MCM-41 particles were incubated in 10 mL of organic solution of pyrene in DCM or hexane, respectively, overnight at room temperature, in which the pyrene concentration was set as 1 $mg\cdot L^{-1}$. After the MCM-41 particles were removed from the pyrene solution and lightly washed with fresh DCM or hexane to remove the pyrene molecules adsorbed on the particle surfaces, they were dried in vacuo at 100 °C overnight and then dispersed in water. The fluorescence spectra of aqueous dispersion of pyrene-borne MCM-41 particles recorded under gentle magnetic stirring to calculate the pyrene-value of the local environment in the MCM-41 mesopores; the pyrene concentration in the aqueous dispersion of pyrene-borne MCM-41 particles was converted from their pyrene loading capacity and set to be 1 $mg\cdot mL^{-1}$. For comparison, the fluorescence spectra of the pyrene solution in water, ethanol and DCM, respectively, were also measured to the pyrene value of these solvents. The pyrene concentration in aqueous and organic solutions was set as 0.1 $mg\cdot L^{-1}$.

1.2.2. Study of the adsorption kinetics and isotherms of MCM-41 particles toward NR in DCM. A series of batch equilibrium adsorption experiments were carried out at room temperature to assess the adsorption performance of MCM-41 particles toward NR in DCM. Freshly cleaned MCM-41 particles were incubated in the DCM solutions of NR molecules and the temporal evolution of the NR concentration in DCM was analyzed by means of UV-vis absorption spectroscopy. The NR adsorption capacity (q^t mg·g^{-1}) of the MCM-41 particles at a given adsorption time (t_a, min) was calculated according to Equation S1:

$$q^t = (C_a^0 - C_a^t)V_a/W_{MCM-41} \qquad \text{(S1)}$$

where C_a^0 (mg·L^{-1}) is the initial NR concentration and C_a^t (mg·L^{-1}) is the NR concentration at a given t_a in DCM, Va is the total volume of the NR solution (10 mL) and W_{MCM-41} is the mass of the MCM-41 particles (40 mg). The C_a^0 is varied from 2 to 4, 5, 10, 15, 20, 25, 40, 50, 62.5, 75, 87.5, 100 mg·L^{-1}.

To reveal the NR adsorption mechanism of MCM-41 particles, the experimentally measured adsorption kinetics data were fitted by pseudo-first-order and pseudo-second-order kinetics models, respectively, according to Equations S2 and S3:

$$\ln(q^e - q^t) = \ln q^e - k_1 t_a \qquad \text{(S2)}$$

$$t_a/q^t = 1/k_2(q^e)^2 + t_a/q^e \qquad \text{(S3)}$$

where k_1 is the rate constant of the pseudo-first-order kinetics model (min^{-1}) and k_2 is the rate constant of the pseudo-second-order kinetics model (g·mg^{-1}·min^{-1}). When the equilibrium adsorption was reached, the equilibrium NR adsorption capacity (q^e, mg·g^{-1}) of the MCM-41 particles was plotted versus the equilibrium concentration (C_a^e) of the NR molecules remained in DCM, described in Equation S4:

$$q^e = (C_a^0 - C_a^e)V_a/W_{MCM-41} \qquad \text{(S4)}$$

The resulting adsorption isotherms were fitted by Langmuir and Freundlich models, repsectively. The Langmuir model is based on the assumption of homogeneous monolayer adsorption on the surface of adsorbents, described in Equation S5:

$$q^e = q^m K_L C_a^e/(1 + K_L C_a^e) \qquad \text{(S5)}$$

where q^m (mg·g^{-1} or mmol·g^{-1}) is the maximum adsorption capacity based on the Langmuir model and K_L (L·mg^{-1} or L·mmol^{-1}) is the Langmuir constant of adsorption. The Freundlich model is based on the assumption of heterogenous adsorption, described in Equation S6:

$$q^e = K_F(C_a^e)^{(1/n)} \qquad \text{(S6)}$$

where K_F and n are the Freundlich constants of adsorption and 1/n is a measure for the sorption intensity.

1.2.3. Preparation of NR-borne MCM-41 particles. After the equilibrium adsorption of NR molecules in DCM was reached, the MCM-41 particles were separated and slightly washed by fresh DCM and dried in vacuo overnight. The NR adsorption capacity (q^e) of the resulting NR-borne MCM-41 particles was altered by the initial concentration of the NR solution in DCM used for incubation.

1.2.4. Study of the TPM extraction performance of pristine and NR-borne MCM-41 particles in aqueous media. Pristine MCM-41 particles were incubated in the PBS solution of TPM dyes, in which the TPM concentration was varied from 0.5 to 30 mg·L^{-1} and the MCM-41 particle mass from 5 to 10 and 15 mg. The temporal evolution of the TPM concentration in PBS was monitored by means of UV-vis absorption spectroscopy; prior to the absorption spectroscopic run, the MCM-41 particles were removed from the TPM solutions by centrifugation at 8000 rmp for 2 min to minimize the scattering effect of the particles.

The similar protocol was applied to study the TPM extraction performance of NR-borne MCM-41, while the particle mass was adjusted to ensure the equivalent mass of the MCM-41 particles was identical. Namely, 5.005, 10.01, and 15.015 mg of NR borne MCM-41 with q^e of 1 mg·g^{-1} and 5.05, 10.1, and 15.15 mg of NR-borne MCM-41 with q^e of 10 mg·g^{-1} were added into the TPM solution in PBS.

1.2.5. Spectroscopic study of the FRET-driven fluorescence quenching of NR molecules in aqueous media in the presence of TPM dyes. 1 mL of the PBS solution of TPM dyes was added into 9 mL of the NR solution in PBS/ethanol (5:4 v/v) mixtures; the NR concentration was set as 1 mg·L^{-1} and the volume ratio of PBS to ethanol volume ratio as 6:4, and the TPM concentration ($\mathrm{C}_{\mathrm{TPM}}^{\mathrm{S}}$) was varied from 1 to 100 mg·L^{-1} in the final solution. The fluorescence intensities at 650 nm of the resulting NR/TPM mixture solutions ($\mathrm{I}_{\mathrm{TPM}}$) were recorded under excitation wavelength of 500 nm with both excitation and emission slits being 1.5 nm.

Similarly, 1 mL of PBS was added into 9 mL of the NR solution in PBS/ethanol (5:4 v/v) mixtures and the fluorescence intensities at 650 nm of the resulting diluted NR solutions (I_0) were recorded. The $\mathrm{I}_0/\mathrm{I}_{\mathrm{TPM}}$ values – fluorescence quenching ratios – were calculated and plotted versus the $\mathrm{C}_{\mathrm{TPM}}^{\mathrm{S}}$ values according to Stern-Volmer equation.

1.2.6. Spectroscopic study of the FRET-driven fluorescence quenching of NR-borne MCM-41 particles in aqueous media in the presence of TPM dyes. NR-borne MCM-41 particles with q^e of 1, 5 and 10 mg·g^{-1} were dispersed in 9 mL of PBS and the particle mass was adjusted to set the NR concentration as 1 mg·L^{-1} the resulting PBS dispersion according to the q^e values. Subsequently, 1 mL of the PBS solution with and without TPM dyes dissolved therein was added into the particle dispersion and the TPM concentration ($\mathrm{C}_{\mathrm{TPM}}^{\mathrm{S}}$) in the final PBS dispersions was varied from 0.1 μg·L^{-1} to 50 mg·L^{-1}. After 1 h incubation under gentle magnetic stirring, the resulting PBS dispersions of NR-borne MCM-41 particles were submitted to fluorescence spectroscopic analysis. The fluorescence intensity at 660 nm in the absence (I_0) and presence ($\mathrm{I}_{\mathrm{TPM}}$) of TPM dyes were under excitation wavelength of 500 nm with excitation slit of 1.5 nm and emission slit of 3 nm and the $\mathrm{I}_0/\mathrm{I}_{\mathrm{TPM}}$ values were calculated and plotted versus the $\mathrm{C}_{\mathrm{TPM}}^{\mathrm{S}}$ values according to Stern-Volmer equation.

1.2.7. Exploitation of NR-borne MCM-41 particles for multiplex FRET-encoded, smartphone-based assay of TPM Dyes in aqueous media. A 3 × 4 plate map was created on a flat bottom microtiter plate, in which the wells in three columns were filled with 1 mg of NR-borne MCM-41 particles with q^e varied from 1 to 5, and 10 $mg \cdot g^{-1}$, respectively, from left to right columns and the wells in four rows were filled by 1 mL of PBS solutions of TPM dyes with C_{TPM}^0 increasing from 0 to 0.01, 0.1 and 1 $mg \cdot L^{-1}$ from bottom to top rows; the wells in the bottom row filled by pure PBS were used as control. After 5 min incubation, the microtiter plate was illuminated by a 10 mW/cm^2 mercury lamp (365 nm) and its fluorescence images were taken by means of a smartphone (Huawei P40). After the the resulting fluorescence images were converted into the 8 bit greyscale images with the help of Image J, the grayscale integrated intensity values of each NR-borne MCM-41 particle/TPM pair-filled well in the microtiter plate were measured and the selected area to register the grayscale intensity values was 1500 pixels.

1.3. Characterization.

UV/vis absorption spectroscopy was carried out on a UV/vis 2700 spectrophotometer (Shimadzu, Japan). Fluorescence spectroscopy was carried out on a fluorescence spectrophotometer (Shimadzu RF5301d, Japan). The fluorescence lifetime and quantum yield of NR molecules dissolved in PBS/ethanol solutions and NR-borne MCM-41 particles in PBS were measured by Edinburgh Instrument FLS920. Nitrogen adsorption-desorption isotherms of pristine and NR-borne MCM-41 particles were measured by ASAP ASAP2020PlusHD88 (Micromeritics Instrument Corp.) and their XRD patterns were recorded by X-ray diffractometer (Empyrean PANalytical B.V.) from 1.5° to 10°. The Fourier transform infrared (FT-IR) spectroscopy of MCM-41 and NR-loaded MCM-41 were characterized by iS 10 Fourier transform infrared spectrometer over a range 400-4000 cm^{-1} (Thermo Fisher Scientific, America), Huawei P40 smartphone was used to take photos under sunlight and UV light and the fluorescence photos of microtiter plates filled with NR-borne MCM-41 particles and TPM solutions were analyzed by means of Image J.

2. Supplementary Data

Figure S1. Summary of the molecular structures of brilliant green (BG), malachite green (MG), methylene blue (MB) and methyl blue. The solubility of BG, MG, MB and methyl blue in water is 40, 40, 43.6 and 70 mg·mL^{-1}.[S1,S2]

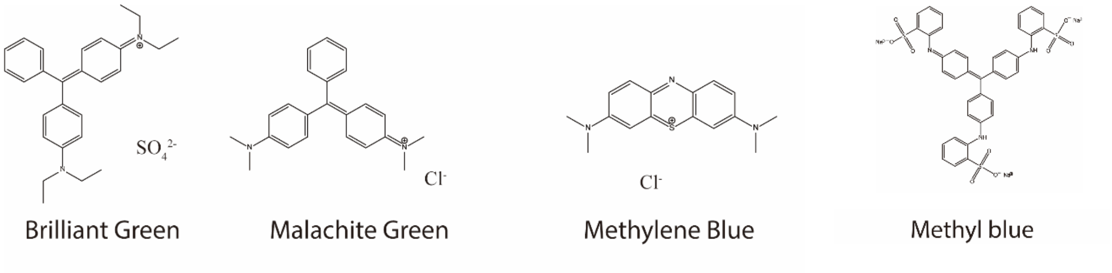

References:

S1. Baughman GL et al,; *Dye solubilities: Advances in Color Chemistry*, Freeman M, Peters MT, eds., NY, NY: Elsevier ,1993.
S2. https://pubchem.ncbi.nlm.nih.gov.

Figure S2. Normalized emission spectrum of NR (black curve), recorded at excitation wavelength of 500 nm (excitation and emission slits of 1.5 nm), and UV-vis absorption spectra of BG (green curve), MG (red curve), and MB (navy curve) in PBS/ethanol mixture solution (6:4 v: v) at the TPM concentration set as 1 µmol·L^{-1}. The spectral overlapping between TPM and NR molecules increases in the sequence of BG, MG, and MB.

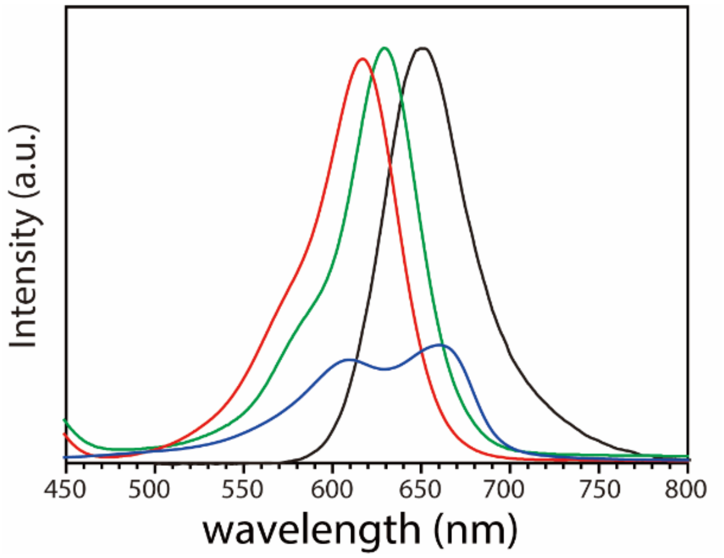

Figure S3. Nitrogen adsorption-desorption isotherms of pristine MCM-41 (a) and NR-borne MCM-41 particles with q^e of 10 mg·g^{-1} (b). The adsorption (black curves) and desorption isotherm data (red curves) are fitted according to Brunauer–Emmett–Teller (BET) theory.

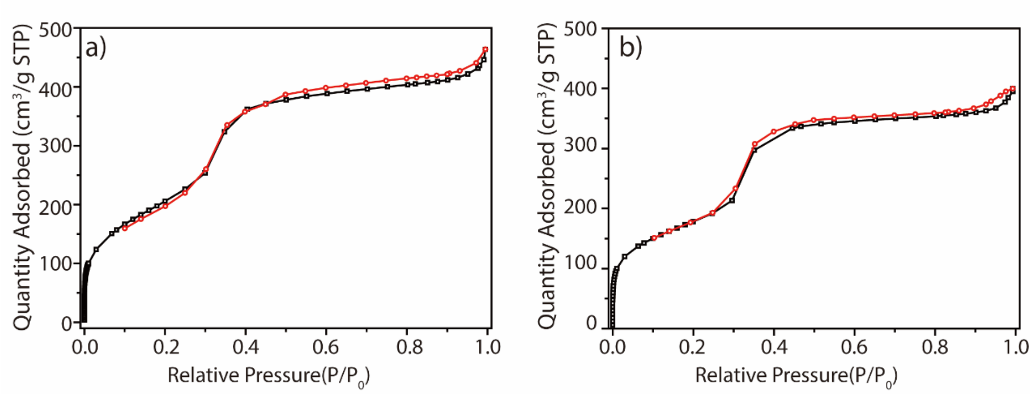

Table S1. Summary of the BET fitting results of the adsorption isotherms of pristine and NR-borne, MCM-41 particles with q^e of 10 mg·g^{-1} shown in Figure S3.

	surface areas (m^2/g)	Pore volume (cm^3/g)	Pore diameter (nm)
MCM-41 particles	780.47	0.717	3.07
NR-borne MCM-41 particles	648.87	0.618	3.05

Figure S4. (a)Fluorescence spectra of pyrene solutions in water (blue curve), DCM (red curves), and ethanol (black curve), respectively, at the pyrene concentration of 0.1 mg·L^{-1}. The intensity ratio of the first emission band at 373 nm (I_{373}) to the third emission band at 384 nm (I_{384}), known as pyrene-values, [S3-S5] are calculated and marked in the Figures, which are 1.61, 1.10 and 0.97 for water, ethanol, and DCM, respectively. (b) Fluorescence spectra of aqueous dispersions of pyrene-borne MCM-41 particles at the equivalent pyrene concentration of 1 mg·L^{-1} converted from the pyrene loading capacity. The pyrene-borne MCM-41 particles are obtained by incubation of freshly cleaned MCM-41 particles in the pyrene solution in DCM (red curve) and hexane (blue curve), whose pyrene values are 1.249 and 1.256, respectively, thus showing little dependence on the operation protocol.

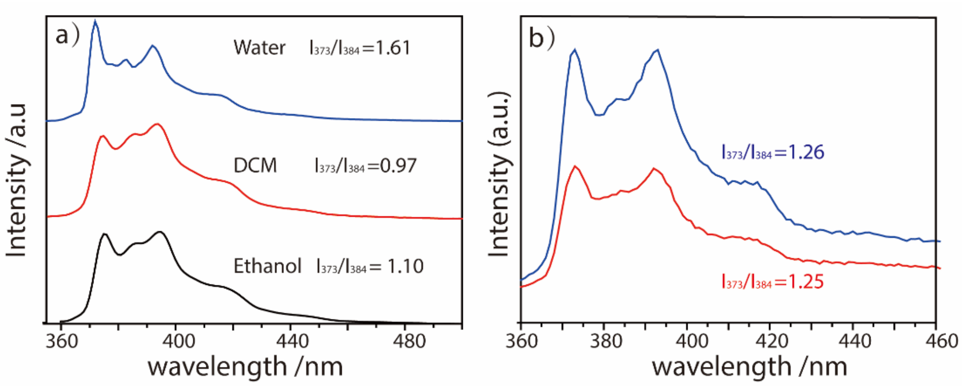

References:

S3. Dong, D.C.;Winnik, M.A.; The Py-Scale of solvent polarities. Solvent Effects on the vibronic fine structure of pyrene fluorescence and fluorescence and empirical correlation with E_t and y Values. *Photochem. Photobiol.* **1982.** *35*,17-21..

S4. Karpovich D S , Blanchard G J. Relating the polarity-dependent fluorescence response of pyrene to vibronic coupling. Achieving a fundamental understanding of the py polarity scale. *J. Phys. Chem.* **1995,** *99*, 3951-3958 .

S5. Tedeschi, C.; Mohwald, H.; Kirstein, S., Polarity of layer-by-layer deposited polyelectrolyte films as determined by pyrene fluorescence. *J. Am. Chem. Soc.* **2001,** *123*, 954-960.

Figure S5. Plots of the concentrations (C_{TPM}) of BG (a), MG (b), and MB (c) molecules in their PBS solutions (10 mL) in the presence of NR-borne MCM-41 particles with q^e of 10 mg·g^{-1} (10 mg) versus incubation time (t). The initial TPM concentration (C^0_{TPM}) in the PBS solution is varied from 1 (black squares) to 5 (red circles) and 10 (blue triangles) mg·mL^{-1}.

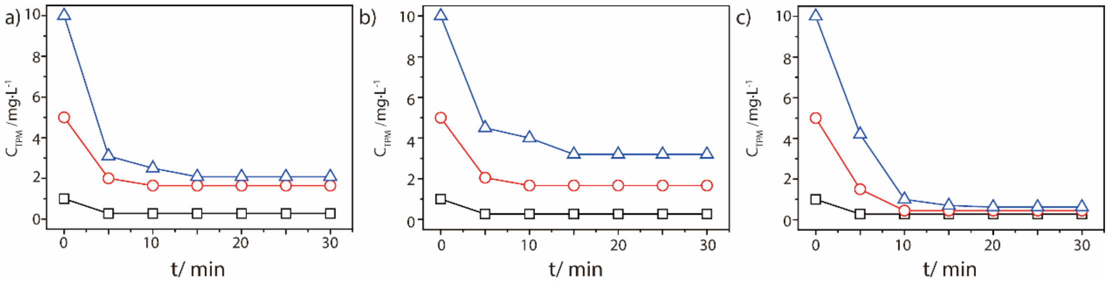

*Note that the temporal C_{TPM} evolution profiles of pristine and NR-borne, MCM-41 particles are almost identical, so here the latter is used instead of the former for better comparison with the TPM-induced fluorescence quenching kinetic data of the NR-borne MCM-41 particles shown in Figure **S19**.*

Figure S5 shows that after MCM-41 particles are incubated in the PBS solutions of TPM dyes for 15 min, the TPM concentration is reduced into the equilibrium value (C^e_{TPM}). Taking into their high-water solubility (Figure S1) and their PBS solution being fairly dilute, the TPM dyes adsorbed on the exterior particle surfaces are expected to be readily dissolved back into the surrounding PBS media. Thus, the TPM concentration reduction should be predominantly assigned to extraction of the dissolved TPM dyes from their aqueous solutions into the less polar mesopores of the MCM-41 particles, which, in turn, can be used to calculate the permeation rate of the TPM dyes into the MCM-41 mesopores. For the sake of simplicity, here the whole exterior surface area of individual MCM-41 particles is used instead of the surface opening areas for calculation, which may hardly alter the order of magnitude of the TPM permeation rate. For a given amount (M = 10 mg) of MCM-41 particles with mean radii (r) of ca. 1.5 μm and mean density (ρ) of 0.7 × 10^3 kg·m^{-3}, the total particle surface area (A) is the sum of the exterior surface area ($S = 4\pi r^2$) of all individual particles, which can be calculate to 2.85 × 10^{-2} m^2 according to Equation (S7):

$$A = [M/(\rho \cdot \tfrac{4}{3}\pi r^3)] \cdot S = 3 \cdot M/\rho \cdot r \qquad (S7)$$

During incubation of 10 mg of MCM-41 particles in a given volume (V_{aq} = 10 mL) of aqueous TPM solution for a given period of time (t) of 900 s (15 min as shown in Figure S5), the permeation flux of TPM dyes into the MCM-41 mesopores can be simply estimated according to Equation S8:

$$\mathrm{J} = [(\mathrm{C}_{\mathrm{TPM}}^{0} - \mathrm{C}_{\mathrm{TPM}}^{\mathrm{e}}) \cdot \mathrm{V}_{aq}]/(\mathrm{A} \cdot \mathrm{t}) \qquad \text{(S8)}$$

In the case of BG, $\mathrm{C}_{\mathrm{TPM}}^{0}$ is 10 mg·L^{-1} and $\mathrm{C}_{\mathrm{TPM}}^{\mathrm{e}}$ is 2.08 mg·L^{-1}, as shown in Figure S5, so its J value is 3.087 × 10^{-9} kg·m^{-2}·s^{-1}. According to Fick's Law, the permeation rate of BG molecules across a given length, defined as $\sqrt[3]{V_{aq}}$, during extraction into the MCM-41 mesopores can be roughly estimated according to Equation S9:

$$\mathrm{D} = \mathrm{J} \cdot [(\mathrm{C}_{\mathrm{TPM}}^{0} - \mathrm{C}_{\mathrm{TPM}}^{\mathrm{e}})/\sqrt[3]{V_{aq}}\,] \qquad \text{(S9)}$$

Hence the BG permeation rate into the mesopores of MCM-41 particles is calculated as 8.40× 10^{-9} m^{2}·s^{-1}. The permeation rates for other TPM dyes are expected in the similar order of magnitude, namely, 10^{-9} m^{2}·s^{-1}.

Figure S6. Plots of the C_{TPM}^{MP} values of TPM dyes accumulated in the mesopores of MCM-41 particles versus the C_{TPM}^{0} values of PBS solutions of BG (black squares), MG (red circles) and MB (blue triangles), respectively, used for incubation of freshly cleaned MCM-41 particles. 10 mL of PBS solution with C_{TPM}^{0} set in the range of 0.5 – 30 mg·L^{-1} are used for incubation of the MCM-41particles.

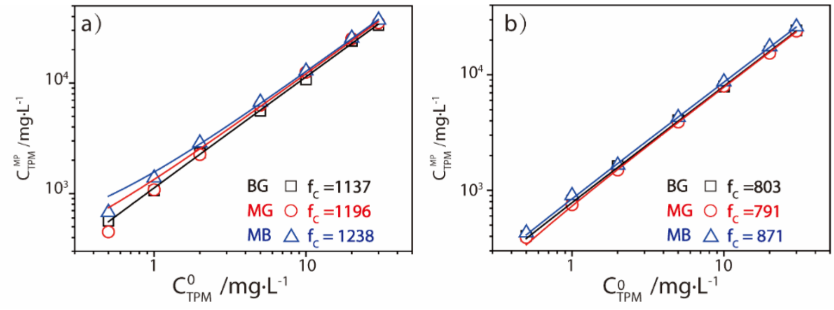

Figure S7. UV-vis spectra of 10 mL of PBS solutions of methyl blue at the concentration of 10 mg·L^{-1} (a) and 30 mg·L^{-1} (b) before (red curves) and after (black curves) 24 h incubation of 10 mg of MCM-41 particles.

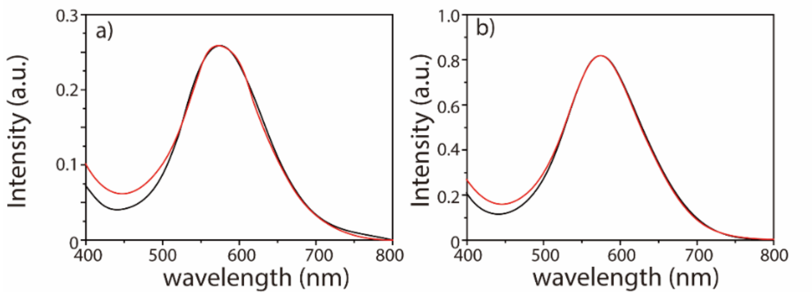

Figure S8. Photos of glass vials containing 5 mL of the PBS solutions of methyl blue, methylene blue (MB), brilliant green (BG), and malachite green (MG), respectively, with 5 mL of octanol placed atop to test the partitioning behavior of these TPM dyes in octanol/PBS biphasic system. In the lower PBS phase, 25 mg of TPM dyes are dissolved therein to form fairly concentrated solutions (2.5 w/w%). All three cationic TPM molecules, MB, BG, and MG show noticeable partitioning in both PBS and octanol phases, evidenced by their color. In contrast, anionic TPM molecules, methyl blue molecules position themselves exclusively in the PBS phase with negligible transfer into the octanol phase, evidenced by the octanol phase remaining colorless.

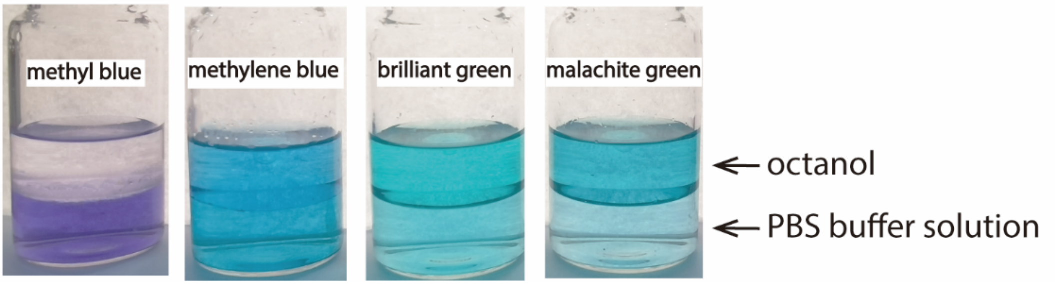

Table S2. Summary of the experimental results of adsorption kinetics of MCM-41 toward NR in DCM and the fitting results obtained based of pseudo-first-order and pseudo-second-order kinetics models

	Pseudo-first-order model				pseudosecond-order model		
C_a^0 (mg·L^{-1})	q^e/exp (mg·g^{-1})	q^e/cal (mg·g^{-1})	k_1 (min^{-1})	r^2	q^e/cal (mg·g^{-1})	k_2 (g·mg^{-1}·min^{-1})	r^2
10	2.345	2.100	0.277	0.749	2.232	0.417	0.836
15	3.498	3.054	0.365	0.646	3.309	0.481	0.759
20	3.902	3.356	0.242	0.69	3.593	0.347	0.805

Table S3. Summary of the equilibrium adsorption uptakes (q^e) of MCM-41 particles toward NR in DCM at different initial NR concentrations (C_a^0).

C_a^0 (mg·L^{-1})	2.0	4.0	5.0	10.0	15.0	20.0	25.0	40.0	50.0	62.5	75.0	87.5	100.0
q^e(mg·g^{-1})	0.53	1.07	1.33	2.64	3.97	5.07	6.13	9.81	11.93	13.46	15.04	15.71	16.79

Table S4. Summary of the fitting results of the adsorption isotherms of MCM-41 towards NR based on Langmuir and Freundlich models in DCM.

Langmuir model			Freudlich model		
q^m (mg·g^{-1})	K_L (L·mg^{-1})	r^2	K_F (mg·g$^{1-1/n}$g^{-1}L$^{1/n}$)	1/n (g·L^{-1})	r^2
17.17	0.40	0.93	6.27	0.29	0.95

Figure S9. Fourier Transfer Infrared spectra of MCM-41 particles (black curve) and NR-borne MCM-41 particles with qe of 10 mg g^{-1} (red curve). The loading of NR molecules cause little change in the FTIR spectra of the MCM-41, indicating that there is no covalent bonds formed between the adsorbed NR molecules and the surfaces of the MCM-41 mesopores.

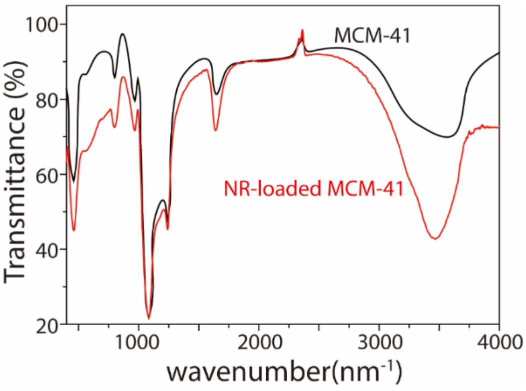

Figure S10. Photos of 2 μL of water drop on the plates of pristine MCM-41 (a) and NR-borne MCM-41particles (b) in air. The plates are prepared by pressing 0.1 g of freshly cleaned pristine MCM-41 particles and freshly prepared NR-borne MCM-41 particles into tables under 2 MPa for 2 min. The water contact angles on the surfaces of the pristine and NR-borne MCM-41 plates are 10.7° and 10.5 °.

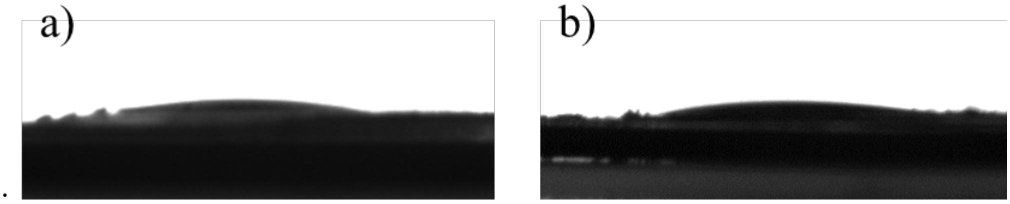

Figure S11. Photograph of a set-up used to record the fluorescence spectra of NR-borne MCM-41 particles under magnetic stirring.

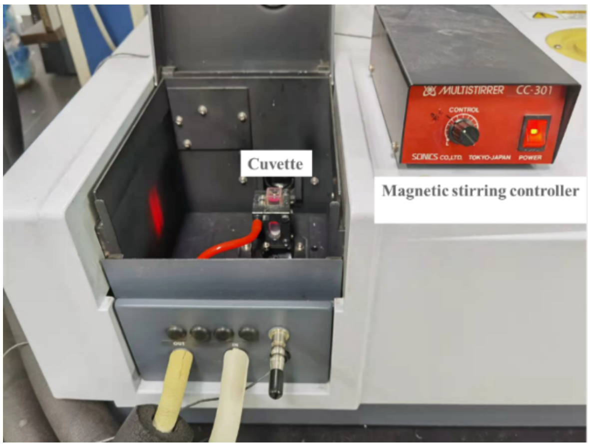

Figure S12. (a) Temporal evolution of the fluorescence spectra of NR-borne MCM-41 particles with q^e of 1 $mg \cdot g^{-1}$, dispersed in PBS recorded immediately after magnetic stirring is turned off. When no magnetic stirring is applied, the particles (of 1 – 2 μm in size) readily participate with time, which leads to no fluorescence observable in the PBS after storage for 24 h. The NR-borne MCM-41 particles can be easily redispersed in PBS with the help of magnetic stirring (Figure S12), enabling the original fluorescence to be completely recovered in the PBS. (b) Plot of the I_0/I ratio of the fluorescence intensity (I_0) of the PBS in which NR-borne MCM-41 particles are well-dispersed under magnetic stirring to that (I) recorded when the particles completely sediment overnight after the magnetic stirring is switched off versus the disperse/sedimentation cycle.

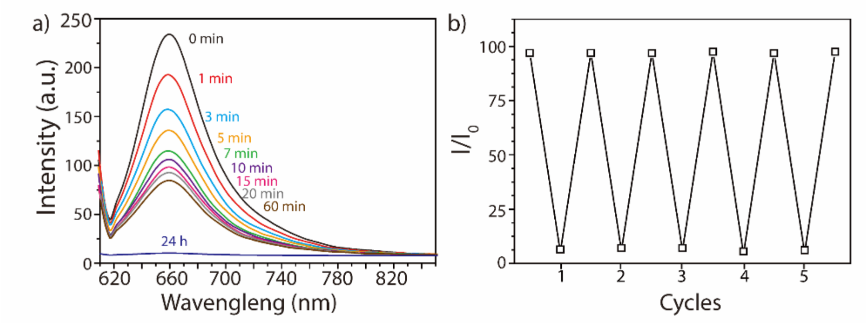

Table S5. Summary of the fluorescence lifetimes (τ) and quantum yields (ϕ) of NR borne-MCM-41 particles with different NR loading capacity (q^e). For comparison, the fluorescence lifetime (τ) and quantum yield (φ) of NR molecules dissolved in ethanol are 3.54 ns and 12 %, respectively

q^e ($mg \cdot g^{-1}$)	τ (ns)	φ (%)
0.5	1.240	5
1	1.738	12
2	1.667	10
5	1.024	6
10	0.704	4

Figure S13. XRD patterns of pristine MCM-41 particles (black curve) and NR-borne MCM-41 particles with q^e of 10 mg·g^{-1} (red curve).

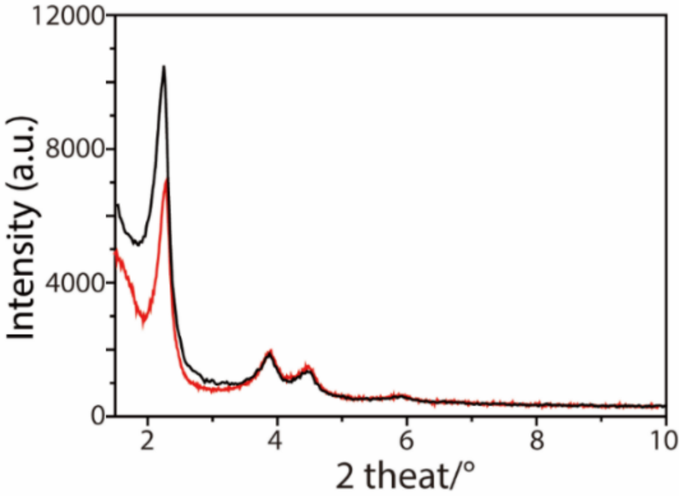

Figure S14. Plots of the C_{TPM}^{MP} values of TPMs accumulated in the mesopores of NR-borne MCM-41 particles versus the C_{TPM}^{0} values of PBS solutions of BG (black squares), MG (red circles) and MB dyes (blue triangles), respectively, used for incubation of the NR-borne MCM-41 particles. 10 mL of PBS solutions with C_{TPM}^{0} set in the range of 0.5 – 30 mg·L^{-1} are used for incubation of NR-borne MCM-41 particles with q^e of 1 mg·g^{-1} (a-c) and 10 mg·g^{-1} (d-f). The particle mass used for incubation is varied from 5 (a, d) to 10 (b, e) and 15 mg (c, f).

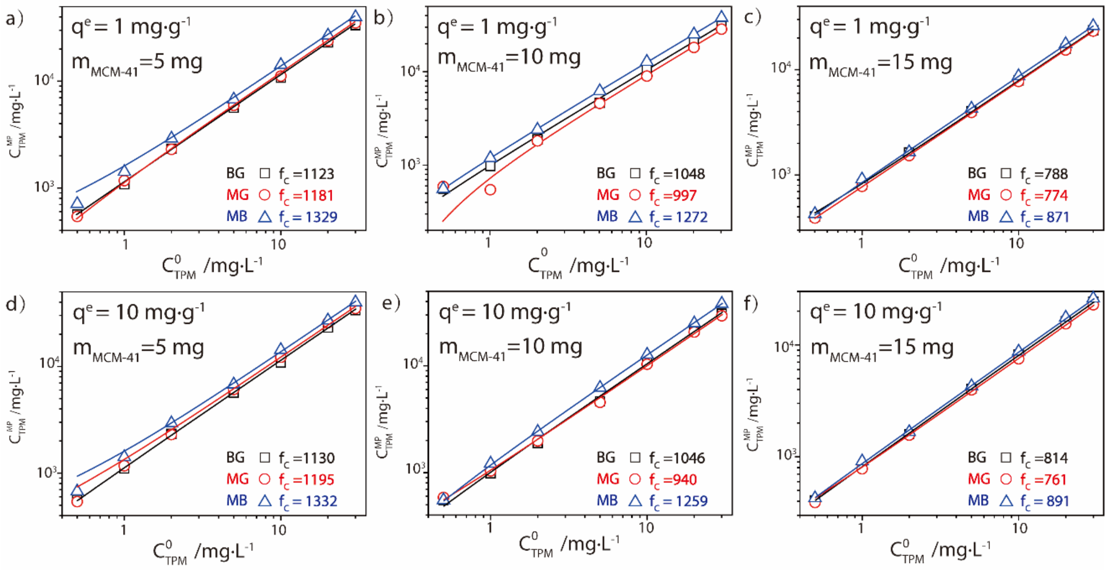

Figure S15. Temporal evolution of the fluorescence spectra of NR molecules dissolved in PBS/ethanol (6:4 v/v) mixtures at the concentration of 1 mg·L^{-1} recorded immediately after addition of BG (a), MG (b) and MB (c) at the concentration varied from 0.1 to 100 mg·L^{-1}. The excitation wavelength of 500 nm and both excitation and emission slits are set as 1.5 nm.

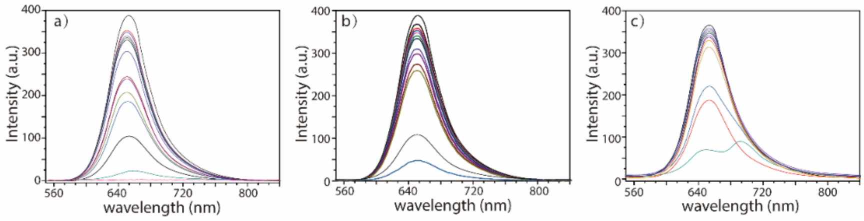

Figure S16. Plots of the I_0/I_{TPM} values at wavelength of 650 nm of NR molecules dissolved in PBS /ethanol (6:4 v/v) mixtures at the concentration of (a, d) 1 mg·L^{-1} (3.14 μmol·L^{-1}), (b, e) 5 mg·L^{-1} (15.7 μmol·L^{-1}) and (c, f) 10 mg·L^{-1} (31.4 μmol·L^{-1}) versus the C_{TPM} values of BG (black squares), MG (red circles) and MB dyes (blue triangles), respectively, added into the PBS/ethanol NR solutions. The C_{TPM} value of TPM dyes in the PBS/ethanol NR solutions are varied from 1 mg·L^{-1} - 100 mg·L^{-1} (a, b, c). Zoom-in portions of the plots, shown in Figures a, b, and c, in the C_{TPM} range of 1 mg·L^{-1} - 10 mg·L^{-1} (3 μmol·L^{-1} – 30 μmol·L^{-1}) are shown in Figures d, e, and f. The excitation wavelength of 500 nm and both excitation and emission slits are set as 1.5 nm.

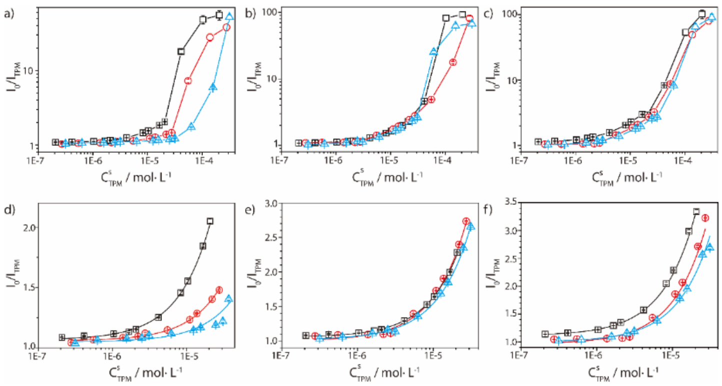

Table S6. Summary of the fluorescence quenching constants (K_{SV}) of NR molecules in PBS/ethanol (6:4 v/v) mixtures at the concentration (C_{NR}) of 1, 5 and 10 mg·L^{-1} ,owing to the NR to TPM FRET. The K_{SV} values are calculated according to Stern-Volmer relationship.

C_{NR}	1 mg·L^{-1} (3.14 μmol·L^{-1})		5 mg·L^{-1} (15.7 μmol·L^{-1})		10 mg·L^{-1}(31.4 μmol·L^{-1})	
TPM dyes	K_{SV}(L·mol^{-1})	r^2	K_{SV}(L·mol^{-1})	r^2	K_{SV}(L·mol^{-1})	r^2
BG	4.650×10^4	0.998	6.283×10^4	0.999	10.834×10^4	0.995
MG	1.575×10^4	0.993	5.800×10^4	0.998	7.516×10^4	0.961
MB	0.837×10^4	0.991	5.275×10^4	0.998	6.070×10^4	0.999

Figure S17. Normalized emission spectrum of the PBS dispersions of NR-borne MCM-41 particles with with q^e of 1 mg·g^{-1} (black curve) recorded at excitation wavelength of 500 nm. With excitation slit of 1.5 nm and emission slit of 3 nm and UV-vis adsorption spectra of the PBS solution of BG (green curve), MG (red curve), and MB (blue curve) at the TPM concentration of 1 µmol·L^{-1}.

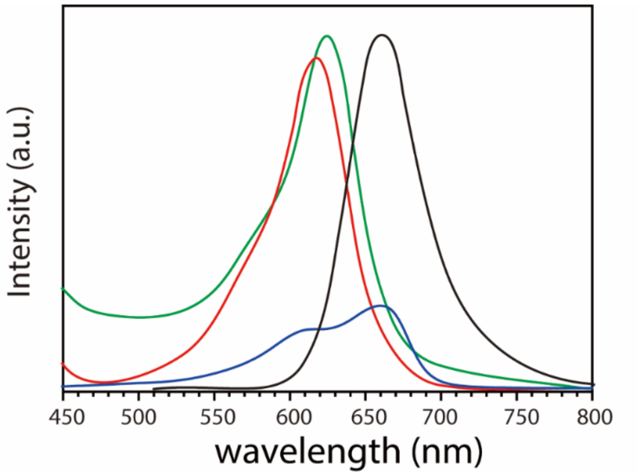

Figure S18. Temporal evolution of the fluorescence spectra of the PBS dispersion of NR-borne MCM-41 particles with q^e of 1 mg·g^{-1} at the NR equivalent concentration of 1 mg·L^{-1} recorded immediately after addition of BG (a), MG (b) and MB (c) at the concentration varied from 0.1 µg· L^{-1} to 50 mg·L^{-1}. The excitation wavelength of 500 nm and the excitation and emission slits are set as1.5 nm and 3 nm, respectively.

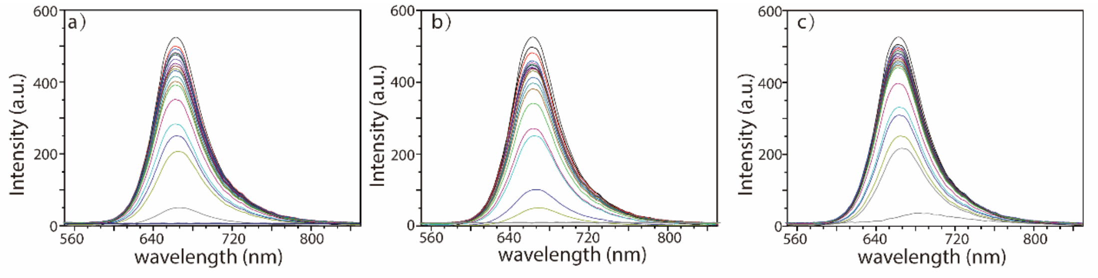

Figure S19. Plots of the fluorescence intensity values at 660 nm of 10 mg of NR-borne MCM-41 particles with q^e of 1 mg·g^{-1} dispersed in 10 mL of PBS in the presence of BG (a), MG (b) and MB (c), respectively, where the TPM concentration is varied 0.1 µg·L^{-1} (black squares), 1 µg·L^{-1} (red circles), 10 µg·L^{-1} (blue upper triangles), 100 µg·L^{-1} (magenta down triangles), 1 mg·L^{-1} (green diamond), 5 mg·L^{-1} (navy left triangles), 10 mg·L^{-1} (violet right triangles), 20 mg·L^{-1} (purple hexagons), and 50 mg·L^{-1} (wine pentagons). The fluorescence spectra are recorded at excitation wavelength of 500 nm with excitation slit of 1.5 nm and emission slit of 3 nm.

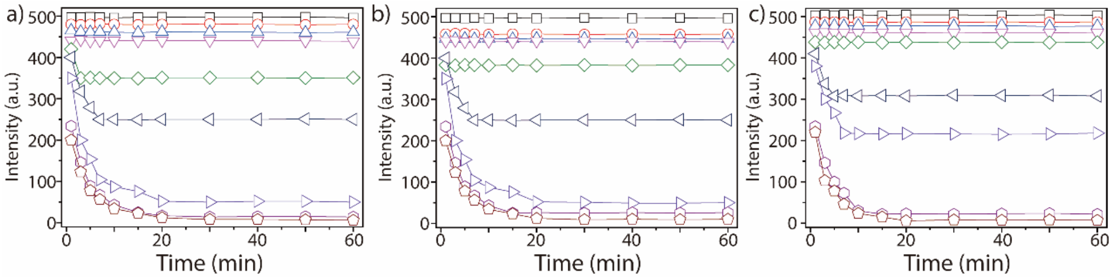

Note that for comparison, the temporal evolution of the TPM concentration in PBS during incubation of the NR-borne MCM-41 particles is shown in Figure S5, which is driven by TPM extraction into the MCM-41 mesopores.

Figure S19 shows that upon addition of TPM dyes in their PBS dispersions, the fluorescence intensity at 660 nm of the NR-borne MCM-41 particles declines and the equilibrium time for the intensity reduction increases from less than 5 min to about 30 min with the TPM concentration (C^0_{TPM}) increasing above 5 mg· L^{-1}. It is plausible to assume that the fluorescence quenching of the NR-borne MCM-41 particles, namely, the fluorescence intensity reduction, occurs only after the TPM dyes permeate into the MCM-41 mesopores to implement the FRET with the NR molecules loaded therein. In this scenario, here the equilibrium time for the fluorescence intensity reduction of the NR-borne MCM-41 particles – 30 min (1800 s) – are used instead of the equilibrium time for TPM extraction into the MCM-41 mesopores to calculate to the permeation flux (J) and rate (D) according to Equations (S8) and (S9); J is 1.57 × 10^{-9} kg·m^{-2}·s^{-1} and D is 2.92 × 10^{-13} m^2·s^{-1} for BG molecules.

Figure S20. Plots of the I_0/I_{TPM} values at emission wavelength of 660 nm of NR-borne MCM-41 particles with q^e of (a, b) 5 mg·g^{-1} (15.7 µmol·g^{-1}) and (c, d)10 mg·g^{-1} (31.4 µmol·L^{-1}) versus the C_{TPM} values of BG (black squares), MG (red circles) and MB dyes (blue triangles), respectively, in PBS. The NR concentration of the NR-borne MCM 41 particles in PBS is equivalent to 15.7 and 31.4 µmol·L^{-1} for q^e of 5 mg·g^{-1} and 10 mg·g^{-1}. The C_{TPM} is varied from 0.1 mg·L^{-1} to 50 mg·L^{-1}(0.3 nmol·L^{-1} – 0.16 mmol·L^{-1}). Zoom-in portions of the plots, shown in Figures a and c, in the C_{TPM} range of 1 mg·L^{-1} - 5 mg·L^{-1}, i.e., 3 nmol·L^{-1} – 16 µmol·L^{-1} , are shown in Figures b and d.

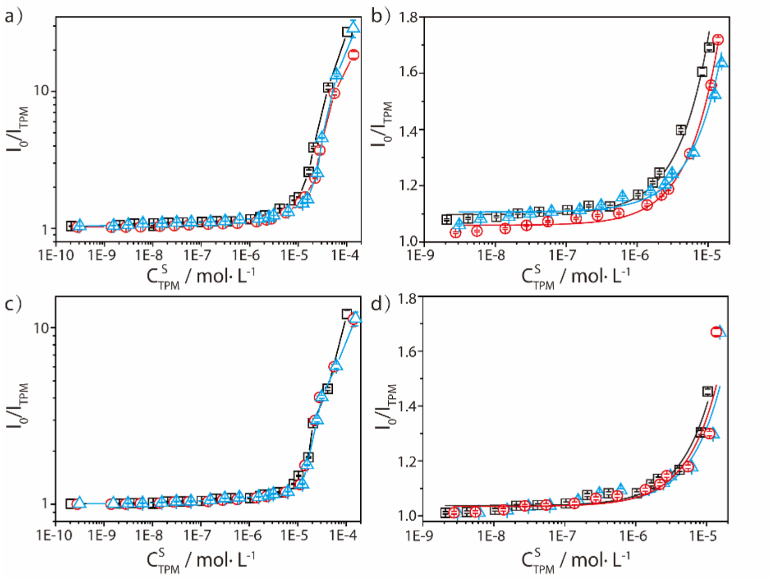

Table S7. Summary of the fluorescence quenching constants (K_{SV}) of NR-borne MCM-41 particles with q^e of 1, 5, and 10 mg·g^{-1} dispersed in PBS in the presence of BG, MG, and MB. The fluorescence quenching data are shown in Figures 4 and S20 and fitted according to Stern-Volmer equation.

q^e	1 mg·g^{-1} (3.14 µmol·g^{-1})		5 mg·g^{-1} (15.7 µmol·g^{-1})		10 mg·g^{-1} (31.4 µmol·g^{-1})	
TPM dyes	K_{SV} (L·mol^{-1})	r^2	K_{SV} (L·mol^{-1})	r^2	K_{SV} (L·mol^{-1})	r^2
BG	8.672×10^4	0.976	6.272×10^4	0.965	3.653×10^4	0.969
MG	4.890×10^4	0.992	3.927×10^4	0.990	3.218×10^4	0.947
MB	5.156×10^4	0.993	3.627×10^4	0.976	2.780×10^4	0.970

Figure S21. (a) Fluorescence spectra of 1 mg·mL^{-1} at 660 nm of 10 mg of NR-borne MCM-41 particles with q^{e} of 1 mg·g^{-1} dispersed in 10 mL of PBS in the presence of different types of organic dyes and (b) Histogram of the corresponding I$_0$/I values (right panel).

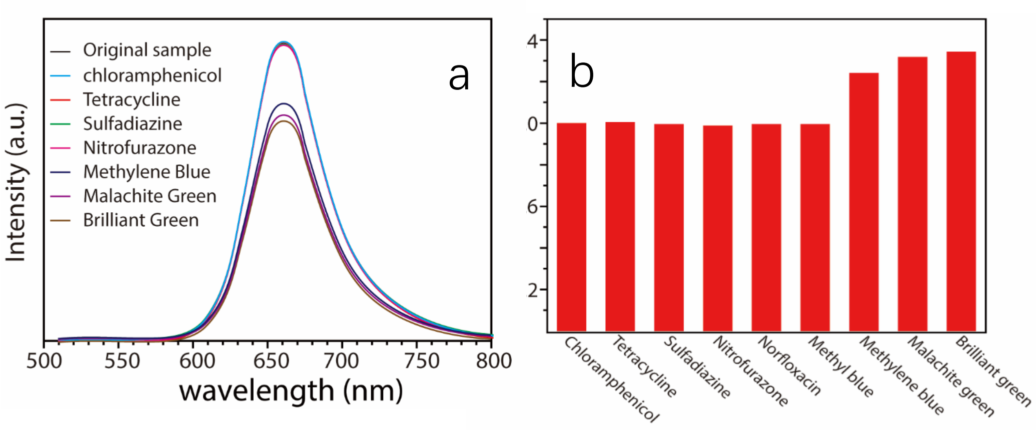

Figure S22. Plots of the I$_0$/I values at 660 nm of NR-borne MCM-41 particles with q^{e} of 1 mg·g^{-1} dispersed in aqueous MG solution (C$_{MG}$) in PBS (upper triangles), fresh fish tank water (circles), lake water (down triangles), and tapwater (squares) at the concentration (C$_{MG}$) varied from 0.1 mg·L^{-1} to 10 mg·L^{-1}, which are fitted according to Stern-Volmer equation.

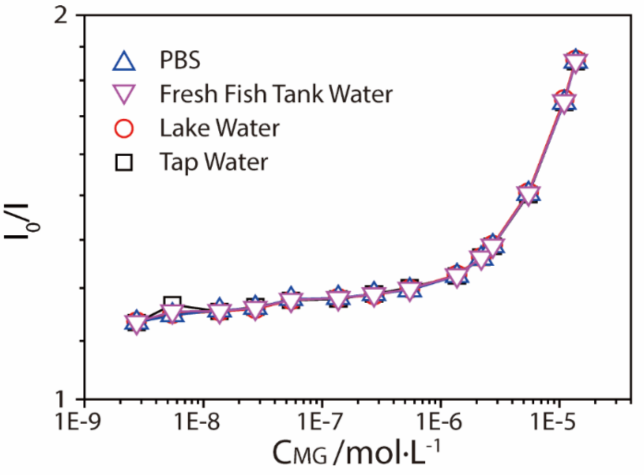

Figure S23. Fluorescence spectra of aqueous solutions of pyrene (0.1 mg·L^{-1}, a) and aqueous dispersions of pyrene-loaded MCM-41 (1 mg·L^{-1}, b) before (black line) and after aqueous MB solution (1 mg·L^{-1}) are added. Excitation wavelength is 340 nm; the excitation and emission slits are set as 3 nm and 3 nm, respectively. Note that MB cause non-negligible fluorescence quenching of pyrene.

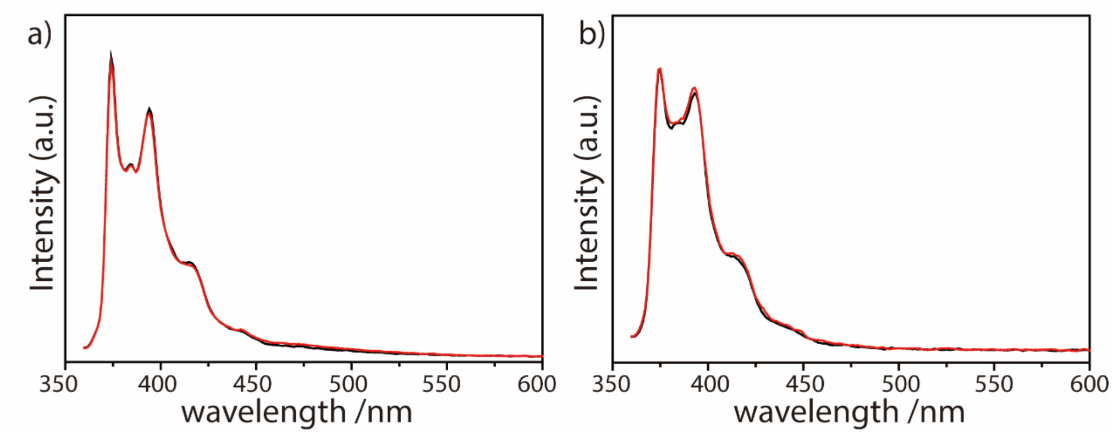

Figure S24. Plots of the recovery percentage of the fluorescence intensity at 660 nm of 10 mg of NR-borne MCM-41 particles with q^{e} of 1 mg·g^{-1}redispersed in 10 mL of fresh PBS after they subsequently underwent the fluorescence quenching by 30 min incubation in 10 mL of the MG solution in PBS, separation from the PBS dispersions and washing by fresh PBS. The MG concentration used for the particle quenching is 0.1 μg·L^{-1} (squares), 1 μg ·L^{-1} (circles), 10 μg ·L^{-1} (upper triangles), 100 μg ·L^{-1} (down triangles), and 1 mg ·L^{-1} (diamonds). The washing time represents the time of repetition of the cycle of separation, washing by fresh PBS redispersion in PBS.

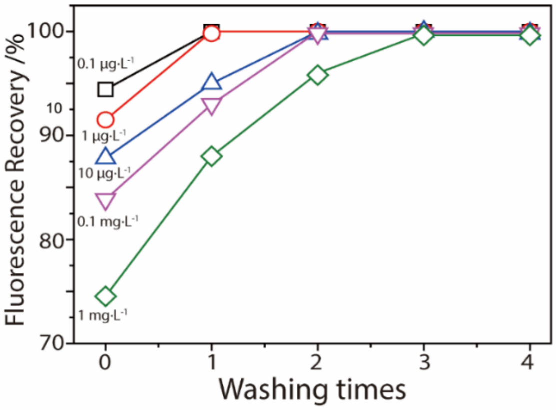

Figure S25. Comparison of the LOQ and linearity range of the present FRET-based arrays with the FRET-based strategies reported in literature. [S6-16]

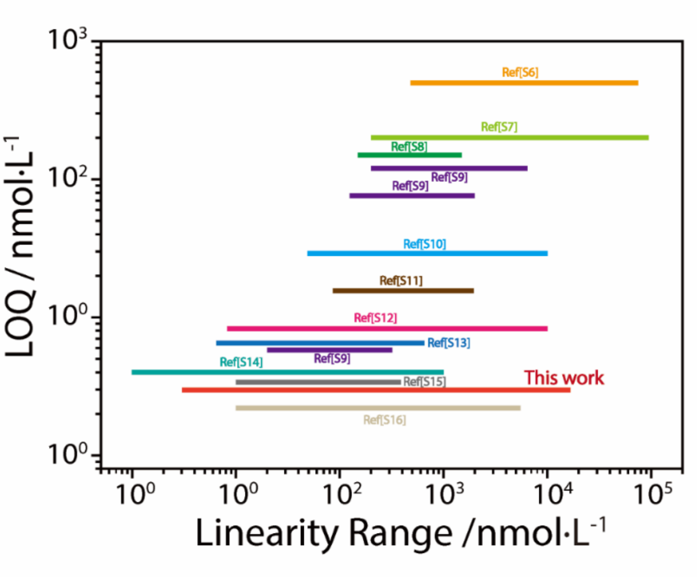

References:

S6. Chen, M.; Chen, R.; Shi, Y.; Wang, J. G.; Cheng, Y. H.; Li, Y.; Gao, X. D.; Yan, Y.; Sun, J. Z.; Qin, A. J.; Kwok, R. T. K.; Lam, J. W. Y.; Tang, B. Z., Malonitrile-functionalized tetraphenylpyrazine: aggregation-induced emission, ratiometric detection of hydrogen sulfide, and mechanochromism. *Adv. Funct. Mater.* **2018**, *28*, 1704689.

S7. Liu, Y. L.; Ai, K. L.; Cheng, X. L.; Huo, L. H.; Lu, L. H., Gold-nanocluster-based fluorescent sensors for highly sensitive and selective detection of cyanide in water. *Adv. Funct. Mater.* **2010**, *20*, 951-956.

S8. Hiremath, S. D.; Priyadarshi, B.; Banerjee, M.; Chatterjee, A. Carbon dots-MnO2 based turn-on fluorescent probe for rapid and sensitive detection of hydrazine in water. *J. Photoch. Photobio. A.* **2020**, *389*, 112258.

S9. Xiao, M.; Liu, Z. G.; Xu, N. X.; Jiang, L. L.; Yang, M. S.; Yi, C. Q., A smartphone-based sensing system for on-site quantitation of multiple heavy metal ions using fluorescent carbon nanodots-based microarrays. *ACS Sens.* **2020**, *5*, 870-878.

S10. Lin, Z. Z.; Li, W. J.; Chen, Q. C.; Peng, A. H.; Huang, Z. Y. Rapid detection of malachite green in fish with a fluorescence probe of molecularly imprinted polymer. *Int. J. Polym. Anal. Ch.* **2019**, *24*, 121-131.

S11. Jouyban, A.; Samadi, A.; Khoubnasabjafari, M. A new "turn-on" fluorescent sensor based on gold quantum dots and silver nanoparticles for lamotrigine detection in plasma. *Talanta* **2017**, *172*, 126-132.

S12. Wang, L. Y.; Dong, L. Y.; Chen, L.; Fan, Y. B.; Wu, J.; Wang, X. F.; Xie, M. X. A novel water-soluble quantum dot-neutral red fluorescence resonance energy transfer probe for the selective detection of megestrol acetate. *New J. Chem.* **2015**, *39*, 555-565.

S13. Louleb, M.; Latrous, L.; Rios, A.; Zougagh, M.; Rodriguez-Castellon, E.; Algarra, M.; Soto, J., Detection of dopamine in human fluids using N-doped carbon dots. *ACS Appl. Nano Mater.* **2020**, *3*, 8004-8011.

S14. Ding, H.; Yi, D.; Liu, F.; Wang, S., Quantitative remote and on-site Hg^{2+} detection using the handheld smartphone based optical fiber fluorescence sensor (SOFFS). *Sens. Actuators B Chem*. **2019**, *301*, 127168.

S15. Sabet, F. S.; Hosseini, M.; Khabbaz, H.; Dadmehr, M.; Ganjali, M. R. FRET-based aptamer biosensor for selective and sensitive detection of aflatoxin B1 in peanut and rice. *Food Chem.* **2017**, *220*, 527-532.

S16. Li, J.; Yang, C.; Wang, W. L.; Yan, X. P. Functionalized gold and persistent luminescence nanoparticle-based ratiometric absorption and TR-FRET nanoplatform for high-throughput sequential detection of L-cysteine and insulin. *Nanoscale* **2018**, *10*, 14931-14937.

Figure S26. (a, b) Photos of a 3 × 4 well microtiter plate with 1 mg of NR-borne MCM-41 particles and 1 mL of PBS solution of (a) MG and (b) MB molecules placed in each well under UV light (left panel) by using a smartphone and converted to 8-bit grayscale image (right panel). The x-axis and y-axis are added into each photo to highlight, respectively, the q^e of the NR-borne MCM-41 particles varying from 1 to 5 and 10 mg·g^{-1} from left to right columns and the $\mathrm{C}^0_{\mathrm{TPM}}$ of the TPM solutions varying from 0 to 0.01, 0.1 and 1 mg·L^{-1} (0.0207, 0.207, 2.075 μmol·L^{-1}) from bottom to top rows. In Figure b the resulting fluorescence RGB image (left panel) is converted to 8-bit grayscale image (right panel) by means of ImageJ. (c, d) Plots of the $\mathrm{G}(q^e, 0)/\mathrm{G}(q^e, \mathrm{C}^0_{\mathrm{TPM}})$ mean values versus the $\mathrm{C}^0_{\mathrm{TPM}}$ values of MG (c) and MB (d) obtained on the 3 × 4 well microtiter plate, which are fitted by Equation (5)

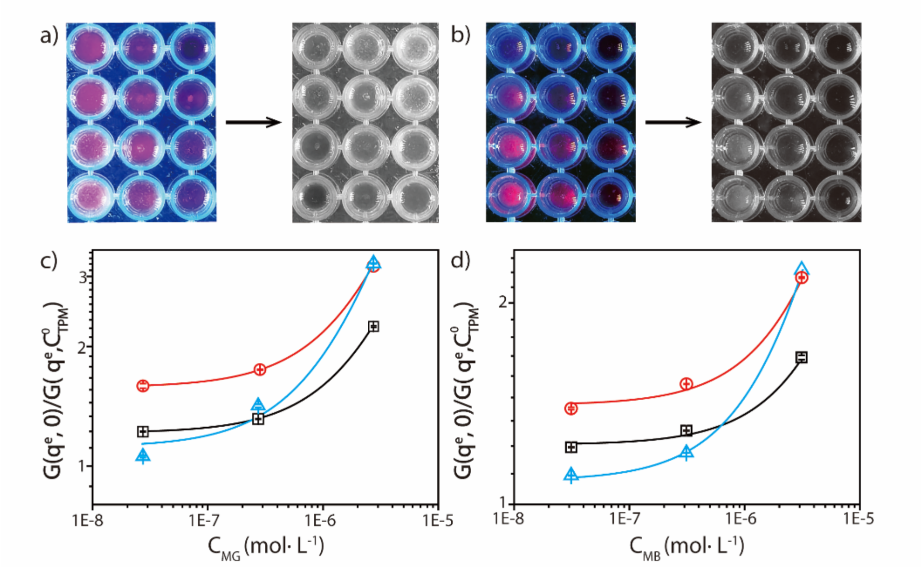

Table S8. Summary of the fitting results of the plots of $\mathrm{G}(q^e, 0)/\mathrm{G}(q^e, \mathrm{C}^0_{\mathrm{TPM}})$ values versus the $\mathrm{C}^0_{\mathrm{TPM}}$ values, obtained on the 3 × 4 well microtiter plate filled with combination of NR-borne MCM-41 particles with q_i^e values of 1, 5, and 10 mg g^{-1} and different types of TPM dyes. The fitting is implemented according to Equation (5).

q^e	1 mg·g^{-1} (3.14 μmol·g^{-1})		5 mg·g^{-1} (15.7 μmol·g^{-1})		10 mg·g^{-1} (31.4 μmol·g^{-1})	
TPM dyes	K$_{\mathrm{GS}}$	r^2	K$_{\mathrm{GS}}$	r^2	K$_{\mathrm{GS}}$	r^2
BG	4.2315×10^5	0.996	2.8970×10^5	0.999	1.5319×10^5	0.998
MG	7.7581×10^5	0.996	5.8838×10^5	0.997	1.7814×10^5	0.990
MB	3.6909×10^5	0.999	2.4832×10^5	0.992	1.3791×10^5	0.990